THE ASTROPHYSICAL JOURNAL, 361:225–234, 1990 September 20

THE X-RAY ABSORPTION SPECTRUM OF VELA X-1

F. HABERL AND N. E. WHITE
EXOSAT Observatory, Space Science Department of ESA, ESTEC, Noordwijk, The Netherlands
Received 1989 October 19; accepted 1990 March 20

ABSTRACT

We present a spectral analysis of all the *EXOSAT* observations of the massive X-ray binary Vela X-1 (4U 0900−40/HD 77581). The absorbing column density shows erratic factor of 10 increases up to 5×10^{23} H cm^{-2} that can occur at any orbital phase and last from minutes to many hours. These variations occur on top of a base level of absorption that increases from 3×10^{22} H cm^{-2} to 15×10^{22} H cm^{-2} from orbital phase, ϕ, $\sim$0.2 to 0.85. The increase in basal absorption after superior conjunction of the X-ray source probably results from the presence of a dense gas stream trailing the neutron star. We suggest the erratic changes in column density are caused by the intermittent formation of a tenuous accretion disk around the neutron star. The X-ray spectra show a low-energy excess above that expected from cold photoelectric absorption. The character of the low-energy excess depends on orbital phase and two different modifications to the simple absorption model are required. Before $\phi \sim 0.5$, when the overall absorption is a minimum, the effects of X-ray ionization of the wind can model the excess. When the column density is higher, both after $\phi \sim 0.5$ and during the erratic absorption events, the low-energy excess is too strong to be modeled as ionization of the wind. It can be well modeled as X-rays scattered by the ambient wind around an absorbing medium that does not completely surround the X-ray source. The X-ray scattering model is confirmed by the fact that during intervals of high absorption the low-energy excess is not pulsed.

Subject headings: stars: accretion — stars: individual (Vela X-1) — stars: neutron — X-rays: binaries — X-rays: spectra

I. INTRODUCTION

Vela X-1 is an 8.96 day eclipsing supergiant X-ray binary system (SXRB) comprising a 23 $M_\odot$ B0.5 Ib star and a neutron star showing 282 s X-ray pulsations (Forman *et al.* 1973; McClintock *et al.* 1976; Rappaport, Joss, and McClintock *et al.* 1976). The pulsar orbits at a distance of $1.7R_*$ ($R_* = 31\ R_\odot$) and is deeply embedded in the supergiants strong stellar wind, causing substantial low-energy photoelectric absorption of the X-ray spectrum (Watson and Griffiths 1977; Kallman and White 1982). The degree of absorption varies with orbital phase and increases toward the time of the eclipse when the neutron star moves behind the dense innermost regions of the wind. An additional absorption component following the neutron star is required to explain a sharp increase in column density after the time of superior conjunction of the pulsar. There are also other intervals when the absorption increases abruptly and erratically lasting from a few minutes to hours (Sato *et al.* 1986). The average X-ray luminosity is $\sim 10^{36}$ ergs s^{-1} and is consistent with that expected from stellar wind accretion onto the neutron star, with no need to invoke an additional gas flow through the Roche lobe (Conti 1978).

The low-energy absorption spectrum of Vela X-1 deviates from that expected from photoelectric absorption. Observations with the *Einstein* solid state spectrometer, SSS, at binary phase 0.2 show an excess below 1.5 keV, indicating that the absorbing medium is partially ionized by the X-ray source (Kallman and White 1982). An SSS spectrum taken at phase 0.75, where the absorption was 3 times higher, shows strong absorption edges near 2 and 2.5 keV. These features are much deeper than expected from neutral absorption and require a reduced opacity at lower energies much greater than expected from photoionization by the X-ray pulsar (Kallman and White 1982). *Tenma* observations by Nagase *et al.* (1986) show a low-energy excess in some X-ray spectra taken during times of high absorption, and Nagase *et al.* (1986) suggest that this excess is due to absorption by clumpy material partially covering the X-ray source. A similar explanation had been proposed earlier for a low-energy excess seen in absorption dip spectra from Cyg X-1, another SXRB (Kitamoto *et al.* 1984).

Spectra obtained during an *EXOSAT* observation of almost one complete binary orbit of the SXRB system 4U 1700−37/HD 153919 also show a low-energy excess (Haberl, White, and Kallman 1989, hereafter HWK). This excess has been classified by HWK into two different types depending on orbital phase and source intensity. When the absorption is a minimum the strength of the low-energy excess is correlated with the source intensity and can be modeled by reduced opacities caused by increased partial ionization of the gas as the X-ray source luminosity increases. During intervals of increased absorption seen at an orbital phase, ϕ, greater than 0.6 a second type of low-energy excess is evident. In this case the strength of the low-energy excess is independent of source intensity and is well modeled as due to scattering of X-rays by the ambient wind around an obscuring gas stream.

We have used *EXOSAT* observations of Vela X-1, made in 1984 and 1985 to investigate the nature of the absorption by the wind of the OB star companion. We find the same two classes of low-energy excess reported by HWK from 4U 1700−37. In § II an overview of the observations is given, including light curves and hardness ratios from the observations. The spectra at various levels of absorption are investigated in § III and the change in the energy dependence of the X-ray pulses during the different levels of absorption presented. § IV presents a reanalysis of the *Einstein* SSS spectra with

respect to the models found for the *EXOSAT* spectra. In § V we test possible models for the low-energy excess. These results are discussed in § VI.

II. OBSERVATIONS

A total of 17 *EXOSAT* observations of Vela X-1 were made at a variety of orbital phases in 1984 February, 1984 December, 1985 February, 1985 April, and 1985 May. A summary of the observations is given in Table 1. The observation duration ranged from 2 to 16 hr. A detailed description of the *EXOSAT* observatory and its instrumentation can be found in White and Peacock (1988). For our study we used the medium energy proportional counter array, ME, sensitive in the 1–20 keV band and the gas scintillation proportional counter, GSPC, sensitive in the 2–15 keV band. To monitor the particle background, one half of the ME array was offset by $\sim 2°$. This excludes the source from the square field of view of $0.°75 \times 0.°75$ FWHM on each side. The GSPC has a factor of 5 smaller effective area as one half of the ME array, but a factor of 2 better energy resolution. Strong solar activity in 1984 February 18, 21, and 23 prevented operation of the ME experiment, but the GSPC was unaffected.

Aspect corrected and background subtracted light curves obtained by the ME in the 0.9–5.0 keV and 5.0–21.0 keV bands from the eight observations made between 1984 December and 1985 May are shown in Figure 1 with a time resolution of 160 s. A hardness ratio obtained from the ratio of the 5–21 keV to the 0.9–5 keV intensity is also shown. Each observation is plotted in order of orbital phase coverage and together cover $\sim 37\%$ of the orbit, albeit from different cycles. Orbital phases were computed using an orbital period of 8.96426 days and a mid-eclipse time (phase 0) of JD 2,445,785.22 (Sato *et al.* 1986). For an inclination of 90° eclipse ingress and egress occur at phase ~ 0.9 and 0.1, respectively.

Even though many of these observations come from different orbital cycles two distinct and repeatable types of variations in hardness ratio are evident. First, there is a base level component that is a minimum at phase ~ 0.25, increases toward eclipse ingress and is repeatable on different orbital cycles. Second, there is an erratically varying component on a time scale of minutes, that lasts from a few minutes to several hours. At early orbital phases ($\phi \sim 0.2$–0.3) the hardness ratio variations range from ~ 1, the minimum value observed, to ~ 4 during the 1985 May 5 observation at $\phi \sim 0.3$. A similar increase in hardness ratio was seen on 1985 May 9 at $\phi \sim 0.73$. Throughout the 1985 May 7 observation ($\phi \sim 0.46$–0.53) the ratio was constant at a high value of ~ 5. At the beginning of the 1985 May 9 observation ($\phi \sim 0.7$) the ratio started lower with a value of ~ 2.5, but half way through the observation it became highly variable increasing at times up to 6. The maximum hardness ratio of ~ 8 occurs during three observations made prior to eclipse ingress on 1984 February 17, 1984 December 18, and 1985 April 22–23.

There is considerable intensity variability on a time scale of minutes throughout many of the observations. The increase in hardness ratio on 1985 May 5 is accompanied by an intensity decrease from ~ 100 counts s^{-1} to ~ 10 counts s^{-1} (0.9–21 keV). Flaring activity is also common with the brightest occurring on 1985 April 22 at 20:45 UT ($\phi \sim 0.86$) where the intensity increased by a factor of ~ 4 over 45 minutes. In many instances there are variations in hardness ratio on a similar time scale to the flares, but mostly with no correlation between the two. One exception was the large flare on April 22 at $\phi = 0.855$ which was preceded 35 minutes and 146 minutes earlier by two unusually large increases in hardness ratio. A cross-correlation of the hardness ratio with the total background-subtracted ME count rate gives peaks at these two time delays, each with a correlation coefficient of ~ 0.4. Two other observations on 1984 December 18 ($\phi \sim 0.87$; the same orbital phase as the observation on 1985 April 22) and 1985 May 9 ($\phi \sim 0.73$) showed also large amplitude variations in the hardness ratio on short time scales (Fig. 1) but with no obvious following flares. A cross-correlation analysis of these two observations does not show a significant correlation between flares in intensity and hardness ratio at any time delay.

TABLE 1

EXOSAT OBSERVATIONS OF VELA X-1

Date	Time (UT)	Orbital Phase	Spectral Mode (N t[a])	Comment
1984 Feb 15	4:59– 8:34	0.59–0.61	32 0.31	
1984 Feb 16	5:45– 9:14	0.71–0.72	32 0.31	
1984 Feb 17	19:29–21:09	0.88–0.89	32 0.31	
1984 Feb 18	10:53–13:03	0.95–0.96	...	eclipse, ME off
1984 Feb 19	5:14– 9:10	0.04–0.06	32 0.31	eclipse
1984 Feb 21	6:23– 8:29	0.27–0.28	...	ME off
1984 Feb 22	7:20– 9:25	0.38–0.39	...	ME off
1984 Dec 18	5:00–16:49	0.84–0.89	128 10	
1985 Feb 11	7:29–17:14	0.99–0.03	128 10	eclipse
1985 Feb 13	6:41–21:30	0.21–0.27	64 1	
1985 Feb 17	4:09–18:42	0.64–0.71	64 1	
1985 Apr 22/23	14:00– 5:26	0.83–0.90	64 1	flare
1985 Apr 30	9:12–17:55	0.70–0.74	64 2	
1985 May 3/4	11:58– 5:32	0.04–0.12	64 2	eclipse
1985 May 5	11:16–21:49	0.26–0.31	64 2	dip
1985 May 7	7:07–20:02	0.47–0.53	64 2	
1985 May 9	9:28–22:35	0.70–0.76	64 2	

[a] The spectra obtained by the ME are binned into N channels with a time resolution given by t in seconds.

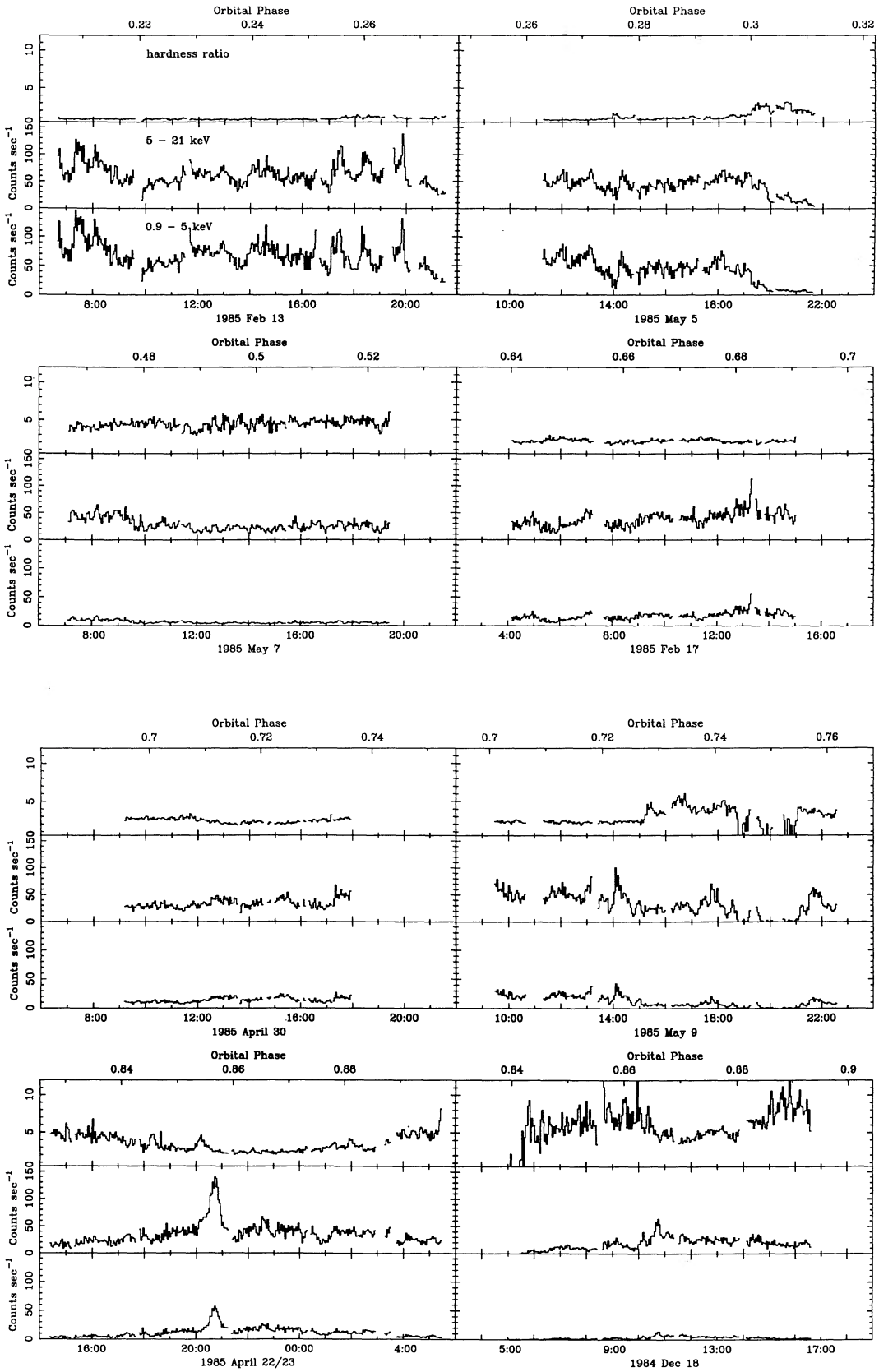

FIG. 1.—Background subtracted light curves of Vela X-1 from the *EXOSAT* observations between 1984 December and 1985 May in the two energy bands 0.9–5 keV and 5–21 keV and the hardness ratio of the two count rates. The count rate is in units of counts per second per half detector array with a time resolution of 160 s. For an overview of all the *EXOSAT* observations see Table 1.

III. THE SPECTRA

a) Overview

The ME PHA spectra were accumulated in either 32, 64, or 128 channels with a time resolution of between 0.31–10 s (Table 1). In our analysis the spectra have been summed into longer time intervals to optimize the signal-to-noise ratio with intervals of 10–50 minutes depending on source intensity. The background was subtracted using spectra from the same detectors offset from the source during nearby time intervals.

The spectra in the energy range 1–21 keV were fit to a power-law model with an energy index α attenuated by neutral absorption. This model has been reported in the past to give an acceptable fit to the spectra (White, Swank, and Holt 1983). In the *EXOSAT* spectra this was not the case, because a low-energy excess was detected below 3 keV, which was particularly prominent during intervals of high absorption. This excess has also been reported by Nagase *et al.* (1986). To study the absorption as a function of orbital phase the fits were restricted to energies greater than 3 keV where an acceptable χ_r^2 was obtained. The derived column density as a function of orbital phase is shown in Figure 2. Different symbols indicate measurements from different binary cycles. Changes in the hardness ratio primarily reflect variations in absorption (see Figs. 1 and 2). The overall column density variations indicate the presence of two absorbing components. There is a base level absorption that is reproduced on different orbital cycles and increases by a factor of ~ 10 from phase 0.2 to 0.85, indicating denser material trailing the X-ray source. In addition there is a highly variable absorption component that appears and disappears at any orbital phase on time scales of a few minutes and can remain from minutes to hours with a maximum absorption of up to 5×10^{23} H cm^{-2}.

b) Low-Energy Excess

To better constrain the nature of the low-energy excess, higher quality ME spectra were accumulated over 3 hr time intervals where the hardness ratio is relatively constant. The fits to the entire spectrum, including the low-energy excess, shows that two different models are required for spectra taken during intervals of low and high hardness ratio. We consider these two cases separately.

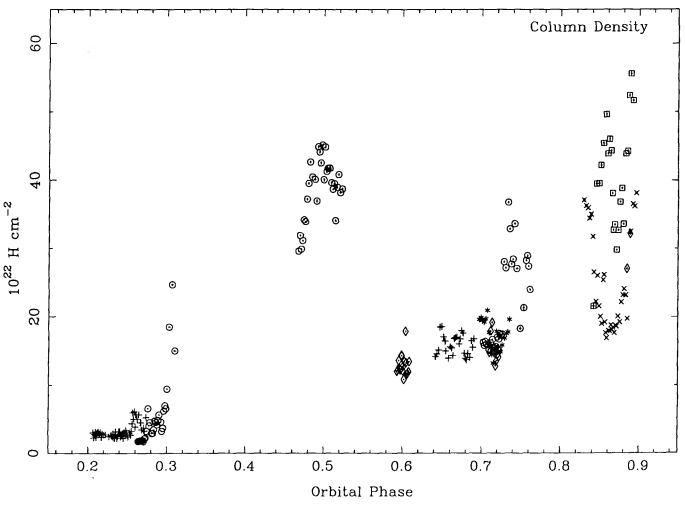

FIG. 2.—Column density derived from fitting a power law plus absorption to the 3–21 keV ME spectra as a function of orbital phase.

Figure 3*a* shows a representative ME spectrum from 1985 May 5 between 14:54 and 17:15 UT ($\phi \sim 0.28$), when the hardness ratio is a minimum (see Fig. 1), together with the best-fitting absorbed power-law model. The overall χ_r^2 is 3.6. The residuals from the model show marked deviations at low energies (Fig. 3*b*). This type of spectral behavior is also evident in the spectra obtained at a similar low hardness ratio (and orbital phase) on 1985 February 13 and on 1985 May 5 (excluding the dip). The X-ray source will ionize the wind in its vicinity and modify the absorption cross sections (Krolik and Kallman 1984). The modification will depend on the distance from the X-ray source. This is approximated with a two-zone model consisting of two absorbing media in series, one with opacities for a photoionized gas and one with neutral opacities (see HWK). This gives an acceptable fit with a χ_r^2 of 0.77 (Fig. 3*c*). For both ionized and neutral gas cosmic elemental abundances are assumed (Morrison and McCammon 1983). The degree of ionization is expressed by the dimension-less parameter $\xi = L_x/nr_x^2$, where L_x is the X-ray luminosity, n is the local wind density and r_x is the distance to the X-ray source (Tarter, Tucker, and Salpeter 1969). The best-fitting ionization parameter, ξ, is $10^{1.64}$ with an ionized column density $N_{\mathrm{H_i}}$ of 21.5×10^{22} H cm^{-2}. The neutral absorption, $N_{\mathrm{H_n}}$, gives only an upper limit of $< 0.5 \times 10^{22}$ H cm^{-2} indicating that the ionized component dominates the absorption. The underlying continuum power-law index, α is 0.44. The residuals from the model, shown in Figure 3*d*, are much improved.

The spectra from observations when the absorption is high also show a prominent low-energy excess, both at orbital phases later than 0.5, and during the erratic hardness ratio increases. Figure 4*a* shows an ME spectrum from 1985 May 7 accumulated from 11:27 to 15:24 UT, together with the best fitting power-law attenuated by neutral absorption. The χ_r^2 is 45 with the residuals from the model fit (Fig. 4*b*) showing a prominent low-energy excess between 1 and 4 keV. Fitting the two-zone model to this spectrum does not give any improvement. Adding a second power-law component with a much lower neutral absorption in parallel with the first does give an acceptable χ_r^2 of 1.2 (Figs. 4*c* and 4*d*). We refer to this as a "parallel absorption model" since a small fraction of the flux reaches the observer with little absorption. The power-law index of the lower N_{H} component is poorly defined, and we fixed it at the same value as the high N_{H} component. The column density of the high N_{H} component is $\sim 7 \times 10^{23}$ H cm^{-2} and for the low N_{H} component is $\sim 2 \times 10^{22}$ H cm^{-2}. The unabsorbed flux of the low N_{H} component is 6% that of the high N_{H} component. This is found in the majority of cases where the parallel absorption model is required. The low-energy excess becomes stronger in the two spectra taken during the dip on 1985 May 5, with the continuum flux in the low N_{H} component 14% and 22% that in the high N_{H} component.

Fitting the parallel absorption model to the low N_{H} spectra at phase 0.2–0.3 (Fig. 3) does not improve the χ^2 significantly, because the shape of the low-energy spectrum is not correct. Combining the two-zone and the parallel absorption models for the low N_{H} spectra at phase 0.2–0.3 slightly improves the χ_r^2 to 0.61 compared to a χ_r^2 of 0.77 for the two-zone model alone.

The higher time resolution 10–50 minutes spectra do not allow both the flux in the low N_{H} component and its column density to be well determined except when the absorption was highest during the observation on 1985 May 7 and on 1985 May 9. To constrain the relative N_{H} of the two components it

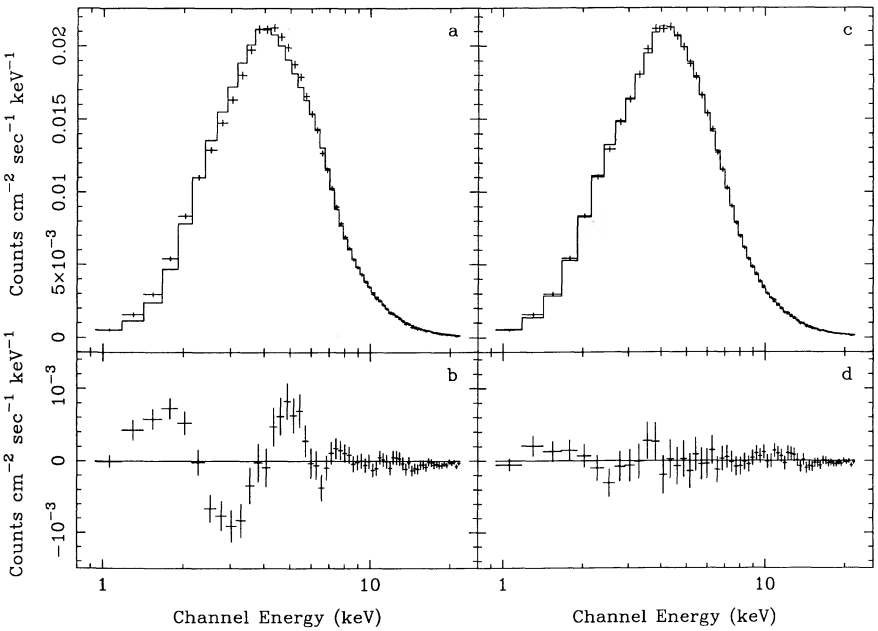

FIG. 3.—An ME spectrum from 1985 May 5 obtained between 14:54 and 17:15 UT. On the left the best-fitting power-law attenuated by photoelectric absorption by neutral material is plotted as a histogram (*a*) together with the residuals (*b*). The same is shown on the right for a two zone model with absorption by ionized and neutral gas in series.

was necessary to fix the normalization of the low N_H component at 5% of the high N_H component, the value found during the majority of intervals where the absorption was high. For those spectra requiring a two-zone model from $\phi \sim 0.2$–0.3 the ionization parameter was also fixed at $\xi = 10^{1.64}$. The N_H of the two absorption components, the power-law index, and the overall normalization were left as free parameters.

Figure 5 shows as a function of orbital phase the direct column density, with the top panel showing the variation in the neutral absorption of the high N_H component, the ionized column density in the middle panel between phase 0.2 and 0.3 where a two-zone model is required and the lower panel the total column density, i.e., the sum of neutral and ionized column density. The neutral and total N_H shows that the increases in hardness ratio are caused by increases in absorption, suppressing the direct low energy flux. The base level N_H increases from 2×10^{22} H cm^{-2} to 15×10^{22} H cm^{-2} with an additional ionized absorption component contributing another 10^{23} H cm^{-2}. Superposed on this are erratic increases in N_H up to 8×10^{23} H cm^{-2}. The absorption variations of the

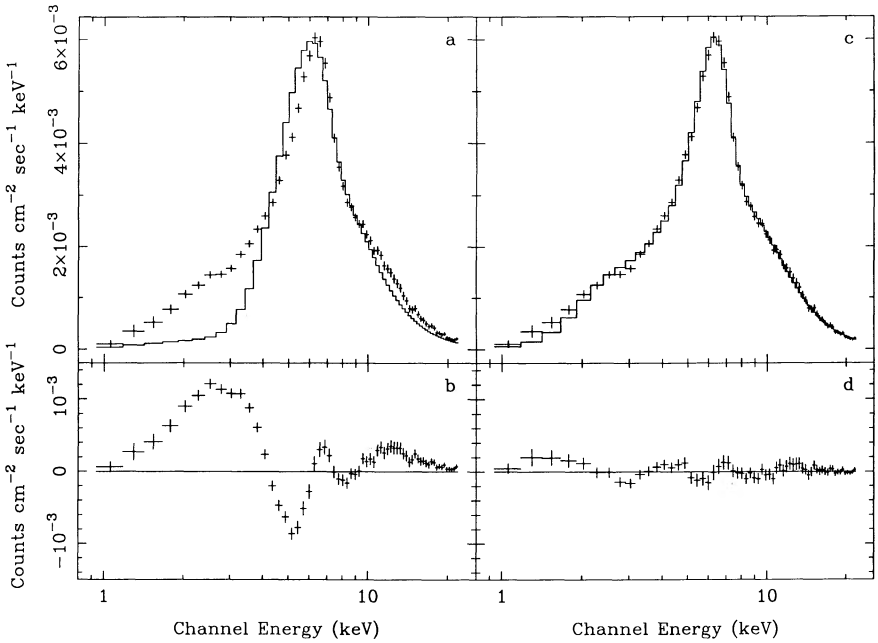

FIG. 4.—On the left an ME spectrum from 1985 May 7 between 11:27 and 15:24 UT is shown with the best fit of a power law as in Fig. 3. The right panels show the best-fitting model comprising of two power-law components in parallel attenuated by different amounts of neutral absorption.

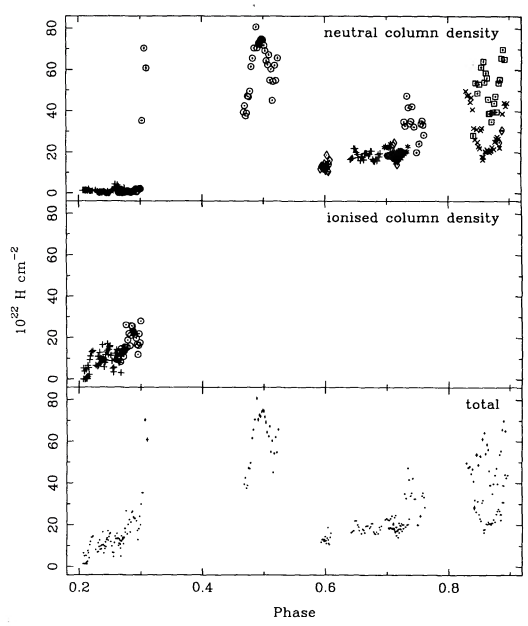

FIG. 5.—In the upper panel the column density of the stronger component derived from fitting two power-law components with different neutral absorption to the ME spectra is plotted as a function of orbital phase. The spectra around phase 0.25 required in addition absorption by ionized gas and the column density for the ionized material is plotted in the middle panel. The total column density along the line of sight is given by the sum of ionized and neutral column density and is plotted in the lower panel.

parallel low N_H component are shown in Figure 6; this component does not show the dramatic changes in N_H seen from its high N_H component companion.

c) *Iron Line*

A narrow iron emission line is required in the fits to the spectra obtained from the GSPC at an energy of between 6.37 ± 0.10 (1985 April 30) and 6.51 ± 0.12 keV (1985 May 9). The line is also required in the fits to the ME spectra, but the factor of 2 lower resolution does not permit such a precise determination of its energy or width. The ME spectral fits use the line energy derived from the GSPC spectra and a FWHM fixed at 0.1 keV. The iron line intensity and equivalent width, EW, depend on which of the two absorption components the line is attached to. We tried both combinations, first with the line attached to the low N_H component and second to the high N_H component. Both give the same χ^2. The left panels of Figures 7*a*–7*c* show the results if the line is added to the low N_H component. The EW (relative to the fainter low N_H component) is constant except for an increase during an intensity dip around $\phi \sim 0.75$ and a single high point close to eclipse ingress. The considerable scatter in the EW around the average is consistent with the uncertainties. The unabsorbed line intensity shows much more variations but these are matched by changes in the total 1–20 keV continuum, e.g., the observation at $\phi \sim 0.6$ (on 1984 February 15) shows the highest line intensity but this corresponds to a flare and the EW is not changed. The line flux and EW does not change during intervals of high hardness ratio. In the right part of Figure 7 the continuum flux (panel *d*), the line flux (panel *e*), and the line EW (panel *f*) are shown for the model where the line is associated with the high N_H component. The higher absorption causes the unabsorbed line intensity to be more than two orders of magnitude higher with the EW (relative to the bright high N_H component) a factor of ~20 lower. The EW increases during periods of high absorption.

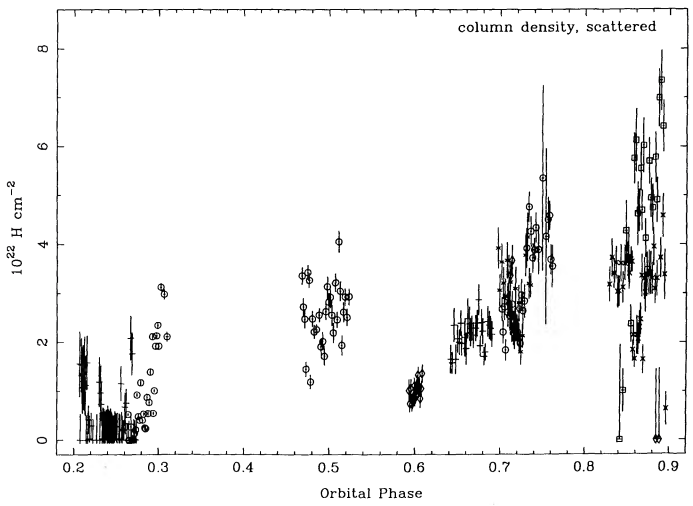

FIG. 6.—Column density of the low N_H parallel absorption component vs orbital phase.

d) *Energy Dependence of the Pulse*

Further information on the origin of the low-energy excess is given by studying the dependence of the amplitude of the X-ray pulsations on absorption. We folded the light curves in two energy bands from 0.9 to 3.6 keV and 3.6 to 21 keV, with the lower band centered on the part of the spectrum where the low-energy excess is most evident. Figure 8*a* shows the pulse profile on 1985 May 5 when the overall absorption was low (excluding the dip after 19:00 UT). The pulse amplitude is normalized to the average counting rate. In the lower energy band the pulse profile is more structured and more deeply modulated as has been reported in the past (see White, Swank, and Holt 1983). Figure 8*b* shows the pulse profile observed in the same two energy bands during the dip that immediately follows, where the low-energy excess was particularly high. In this case the low-energy amplitude is much reduced, whereas in the high-energy band the pulsations are unchanged. The same reduction in the amplitude of the low-energy pulse is visible during all observations where the overall N_H is high. Another example is the observation on 1985 May 7 shown in Figure 8*c* with again very little low-energy pulsations, compared to the higher energy band. There is a very small amplitude residual pulsation that has the same structure as the higher energy pulse. This residual is from the small amount of the absorbed direct component that still leaks into the low-energy band.

IV. THE *EINSTEIN* SSS SPECTRA

We have reanalyzed the Vela X-1 spectra from the *Einstein* SSS in 1979 (Kallman and White 1982) at $\phi \sim 0.19$ and 0.75. A single power-law model with neutral absorption gives an acceptable fit to the $\phi \sim 0.19$ spectrum with a χ^2_r of 1.3, $N_H = 2.9 \times 10^{22}$ H cm^{-2} but with an α of -0.15, lower than the value of 0.3–0.4 found by *EXOSAT*. The fit to the $\phi \sim 0.75$ spectrum is also acceptable but gives a α of -4.8 with no absorption required. The energy range covered by the SSS is not wide enough to restrict the power-law index in these highly absorbed spectra. When the power-law index is fixed at the value of 0.33, found for the *EXOSAT* ME spectra, the natural

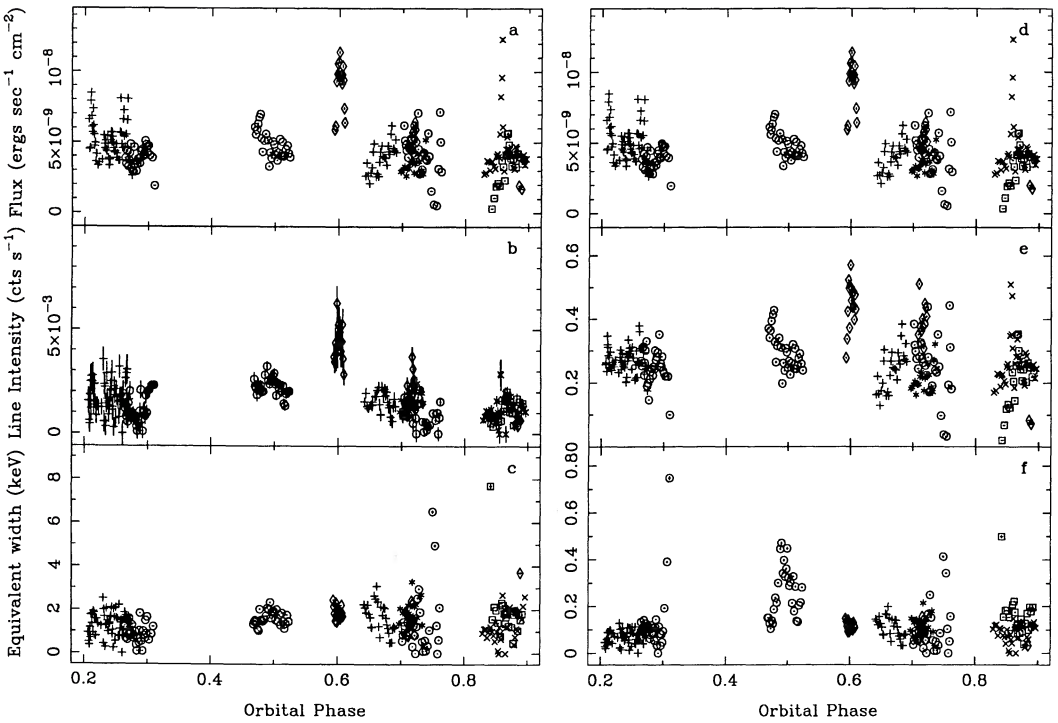

FIG. 7.—Spectral properties for the Vela X-1 spectra with an iron fluorescence line added to the low N_H component (*left three panels*) or added to the high N_H component (*right three panels*) of the parallel absorption model shown vs. orbital phase. In (*a*) and (*d*) the total flux in the 1.0 to 20.0 keV band and in (*b*) and (*e*) the unabsorbed line intensity is plotted. In panels *c* and *f* the line equivalent width calculated using respectively the low N_H component and the high N_H component as continuum is shown.

absorber model gives unacceptable fits. The two-zone model gives an acceptable fit to the $\phi \sim 0.19$ spectrum with a χ_r^2 of 1.0, a neutral column density $N_H = 1.7 \times 10^{22}$ H cm^{-2}, an ionized column density $N_H = 17.5 \times 10^{22}$ H cm^{-2} and an average ionization parameter, $\xi = 10^{1.68}$. This fit is shown in the upper panel of Figure 9. The parameters are all consistent with those found from the *EXOSAT* ME spectra. This confirms the suggestion by Kallman and White (1982) that photoionization is the reason for the low-energy excess they found. The parallel absorption model was fitted to the $\phi \sim 0.75$ spectrum and gives an acceptable χ_r^2 of 1.1. The column density of the low N_H and the high N_H components are 2.9×10^{22} H cm^{-2} and 24×10^{22} H cm^{-2}, respectively. The total continuum flux in the low N_H component is 3% of that in the high N_H component, again similar to the *EXOSAT* spectra from intervals of high N_H. The best fit is shown in the lower panel of Figure 9. The $\phi \sim 0.75$ spectrum below 3 keV is dominated by the low N_H component. The Si and S edges may be more pronounced in the data than in the model, but not significantly so, since the χ^2 is acceptable.

V. THREE ABSORPTION COMPONENTS

We find that three absorption components are required to explain the spectra of Vela X-1 observed by *EXOSAT*. In all spectra there is a highly variable neutral absorber that obscures the central pulsar. When this neutral absorption component is close to its minimum value the effects of partial ionization of material close to the X-ray source become visible and a second ionized absorption zone is required. During intervals of high absorption a third low absorption component, in parallel with the other two, is required with a flux typically 5% that of the highly absorbed component, although on one occasion it was as high as 22%.

Nagase *et al.* (1986) have reported a similar low-energy excess in the spectra of Vela X-1 and also fit a similar parallel absorption model. They interpret the low N_H component as resulting from partial covering of the X-ray source and infer the presence of high-density bullets in the wind with a scale of 20 km or less, i.e., less than the diameter of a neutron star. In this model pulsations from the neutron star should be detected at low energies, contrary to our observation that the low-energy excess is not pulsed.

The lack of low-energy pulsations suggests instead the scattering model we proposed to explain a similar low-energy excess from 4U 1700−37 (HWK). In this model the high N_H component arises from the X-ray source obscured behind a gas stream or dense material in the wind, and the low N_H component are X-rays scattered by the ambient wind. Because these are scattered X-rays, the pulsations are smeared out.

The ratio of the overall continuum flux in the low and high N_H components can be used to investigate the geometry. At the upper end of the range of column densities measured from Vela X-1 the Thomson optical depth approaches unity and will scatter a fraction of the X-rays out of the line of sight. The ambient stellar wind also scatters a smaller fraction of the X-ray flux back into the direction to the observer. The magnitude of these effects depend on the geometry and distribution of the material in the wind. The absorption cross sections used in the spectral fits do not include the energy independent Thomson electron scattering and so part of the reduction in flux in the direct component is caused by this. In the upper and lower panel of Figure 10 the observed ratio of the continuum flux in the scattered (low N_H) component to that in the direct (high N_H) component is plotted against the ratio of the column density of the direct to the scattered component for the 1985 May 5 and 7 observations ($\phi \sim 0.3$ and 0.5) when the absorp-

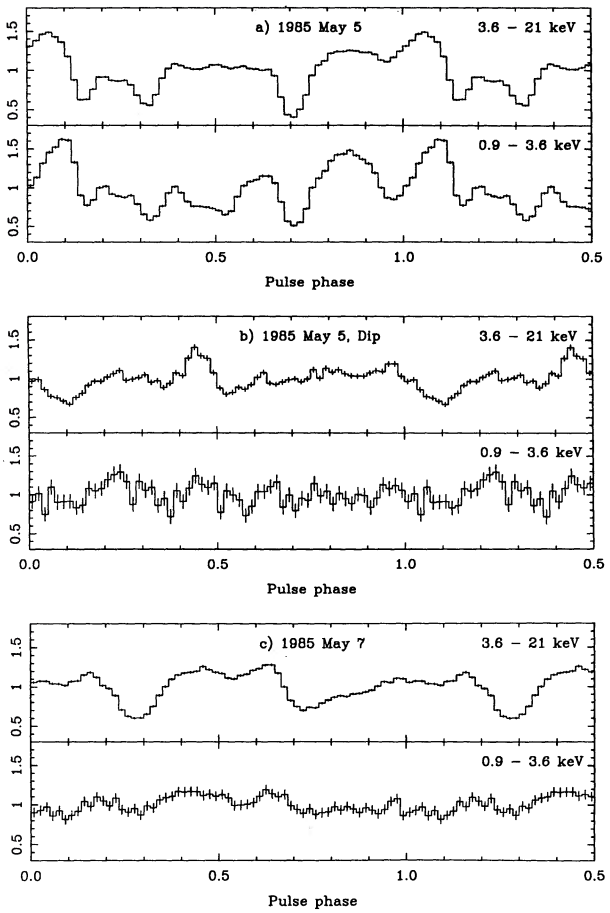

FIG. 8.—X-ray light curves folded with the pulse period in two different energy bands and plotted vs. an arbitrary pulse phase. While during the observation on 1985 May 5 (excluding the intensity dip at the end of the observation) the pulse profile shows pronounced maxima and minima in both energy bands, during the dip almost no pulsations are present in the low-energy band. Also during the May 7 observation which shows a strong low-energy excess in the spectra little pulsations are visible at energies below 3.6 keV.

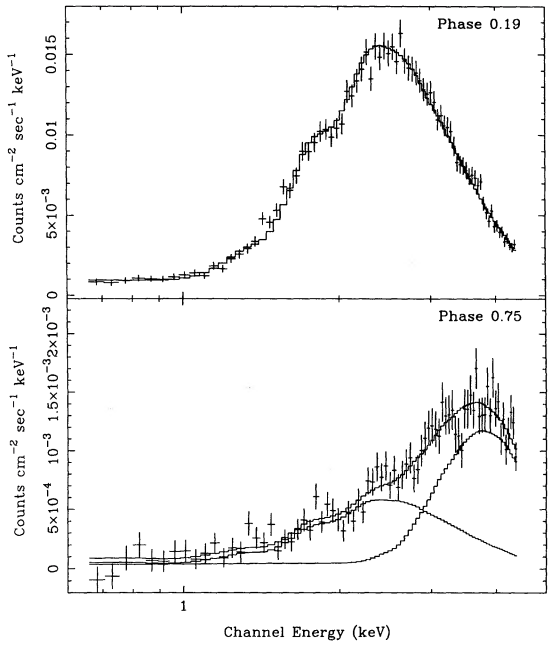

FIG. 9.—Two *Einstein* SSS spectra observed in 1979 by Kallman and White (1982) around binary phase 0.19 and 0.75. The two-zone model gives a good fit to the phase 0.19 spectrum. The highly absorbed spectrum from phase 0.75 is modeled using the parallel absorption model.

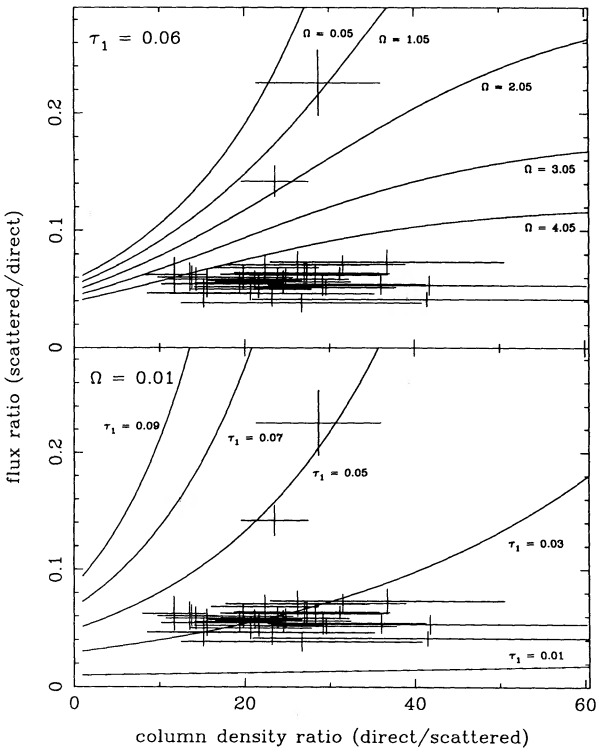

FIG. 10.—The intensity ratio of the two power-law components fitted to the dip spectra from 1985 May 5 (*upper two crosses in upper and lower panel*) and the spectra from 1985 May 7 (*lower crosses*) are plotted vs. the ratio of the two column densities for the two components derived from the spectral fitting. The solid lines are derived using a model for Thomson scattering in a sphere of optical depth τ_1 and τ_2 in a cone along the line of sight. In the upper panel the ratio of the emerging components is plotted vs. the ratio of τ_1 and τ_2 for a τ_1 of 0.06 using different solid angles Ω covered by the cone. In the lower panel a value of 0.01 is used for Ω while τ_1 varies between 0.01 aand 0.09. The model assumes that the electron column density is equal to the hydrogen column density responsible for the photoelectric absorption.

tion was high. Most of the points lie with a flux ratio of ~0.05 and a wide range of column density ratio. The two upper data points with a flux ratio of 0.14 and 0.22 are from the dip spectra on 1985 May 5. The higher intensity ratio for these points illustrates the higher scattering fraction mentioned earlier.

To understand the geometry of obscuring and scattering region, the scattered flux has been modeled assuming a uniform sphere with a Thomson optical depth τ_1 surrounding the X-ray source, plus an additional Thomson optical depth τ_2 ($\tau_2 \geq \tau_1$) along the line of sight in a cone subtending a total solid angle Ω. The electron column densities given by τ_1 and τ_2 are equal to or greater than the equivalent value of N_H measured for the low and high N_H components in the parallel absorption model. They will be greater if there is a highly ionized zone close to the X-ray source, where the low-energy absorption is reduced. Secondary scattering in the two regions will be neglected (this will be negligible for $\Omega \ll 4\pi$ and $\tau < 1$).

The solid lines in the lower panel of Figure 10 show the predicted ratio of the flux in the low absorption to the high absorption component for values of τ_1 ranging from 0.01 to 0.09 in steps of 0.02 [equivalent to $N_H(\tau_1) = 1.5 \times 10^{22}$ H cm^{-2} to 13×10^{22} H cm^{-2}, the range covered by the observed values] for Ω fixed at the small value of 0.01. The relative

strength of the low-absorption component is very sensitive to τ_1, and for $\Omega = 0.01$ requires $\tau_1 \sim 0.05$ to account for the high intensity of the scattered low-absorption component. For the dip spectrum where the flux ratio is 14% the column density ratio is -23. The high scattered flux requires an equivalent $N_H(\tau_1)$ of $\sim 7.5 \times 10^{22}$ H cm^{-2} and with the column density ratio $N_H(\tau_2)$ of 1.7×10^{24} H cm^{-2}, which is ~ 2.5 times larger than the observed values of 3×10^{22} H cm^{-2} and 7×10^{23} H cm^{-2}. An unknown is the magnitude of any additional scattering in the ionized region; this will effectively increase τ_1.

The upper panel of Figure 10 shows the flux ratio for values of Ω ranging from 0.05 to 4.05 for $\tau_1 = 0.06$ [equivalent to $N_H(\tau_1) = 9 \times 10^{22}$ H cm^{-2}]. The smaller the solid angle subtended by the region of high density, the larger the fraction of emission in the scattered low N_H component. For larger Ω, the flux ratio will be overestimated because X-rays scattered in the τ_1 region will be absorbed in the τ_2 region and contribute to the high-absorption component. The dip seen on 1985 May 5, where the scattered component is exceptionally large (and also some of those reported earlier by Nagase *et al.* 1986), requires either an increase in τ_1 or a decrease in Ω. A change in τ_1 seems unlikely as this requires a global change in the overall structure of the wind on a very short time scale. The passage into the line of sight of a dense region that subtends a small solid angle is more plausible.

In Figure 11*a* each absorption spectral model component is plotted assuming $\Omega = 0.01$ for $\tau_1 = 0.02$ [equivalent to the observed value $N_H(\tau_1) = 3 \times 10^{22}$ H cm^{-2}] and $\tau_2 = 0.47$ [observed $N_H(\tau_2) = 7 \times 10^{23}$ H cm^{-2}]. Component 1 is the direct high N_H component, component 2 the part scattered into the line of sight inside the high N_H cone, and component 3 the scattered part from the rest of the low N_H scattering sphere. The unabsorbed intrinsic X-ray source spectrum is also shown as the upper solid histogram. The observed spectrum from the dip on 1985 May 5, when the low energy excess was 14%, is plotted as crosses. The model predicts a spectrum that falls well below the data. In Figure 11*b* the same model is shown with $\tau_1 = 0.08$, a factor of 4 higher than expected from the observed equivalent hydrogen column density. The model is in good agreement with the data. This additional scattering (energy independent) column density is consistent with that expected in the zone of highly ionized material which is visible during intervals of low N_H. This requires an equivalent N_H of up to 2×10^{23} H cm^{-2} in the ionized zone and is equivalent to a Thomson depth of up to 0.14.

The spectra from the base level absorption from phases later than 0.4 have a weaker low-energy excess compared to the dip spectra with, e.g., the spectra on 1985 May 7 requiring a factor of 3 higher Thomson optical depth than the equivalent hydrogen column density, compared to 4–8 during the dip. This suggests that the high-absorption dips are caused by a smaller obscuring region, subtending a smaller solid angle.

VI. DISCUSSION

The shape and variability of the low-energy spectrum of Vela X-1 shows two deviations from a simple neutral absorption model. When the base level absorption is a minimum at the earliest orbital phases (0.2–0.3), the ionizing effects of the X-ray source on the wind must be included. When the absorption is higher both at later orbital phases and during erratic absorption events, X-rays scattered around the obscuring medium by the ambient wind is important.

The effects of X-ray ionization on the wind was modeled

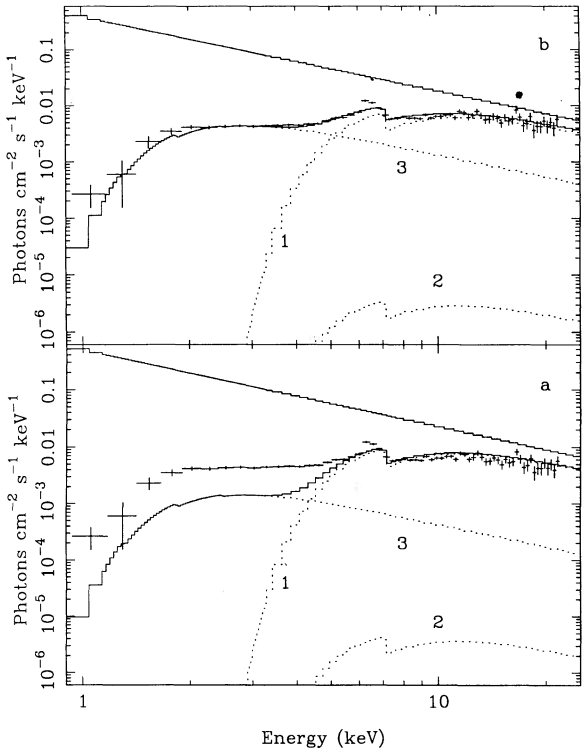

FIG. 11.—The dip spectrum from 1985 May plotted as photon spectrum. Using the scattering model from Fig. 10 the components of the emerging spectrum (*lower solid histogram in both panels*) are shown. Component 1 is the direct beam highly absorbed by the cone of dense material. Component 2 is the inside the cone scattered part toward the observer and 3 the scattered X-rays from the rest of the less absorbing sphere. The intrinsic source spectrum is also plotted (*upper solid histogram in both panels*). The absorbing hydrogen column densities for the two components are taken from the best fit to the dip spectrum and are 3×10^{22} H cm^{-2} and 70×10^{22} H cm^{-2} for the sphere and the cone respectively. The lower panel shows the model assuming equal electron and hydrogen column densities. In the upper panel a factor of 4 higher electron density for the scattering sphere is used.

using the HWK two-zone model to fit a low-energy excess seen in flare spectra of 4U 1700−37. An ionization parameter ξ of $\sim 10^{1.65}$ in the ionized zone is found for Vela X-1, similar to the value of $10^{1.6}$ found for 4U 1700−37 (see HWK). In 4U 1700−37 the fraction of the absorption caused by the ionized zone increases as the source flares. The dynamic range of the flares from Vela X-1 is not sufficient to detect a similar effect. A two-zone model is an idealization to approximate a smoothly changing ionization structure. Adding additional zones does not give any improvement in an already acceptable χ^2 and reflects the poor energy resolution of a proportional counter which cannot resolve individual L and K photoelectric absorption edges.

When the absorption is high the low-energy excess can be modeled as emission scattered by the ambient wind around an obscuring medium. This suggests that the intervals of higher N_H, both in increasing base level absorption at orbital phases greater than 0.5 and in the erratic increases in absorption do not completely surround the X-ray source, but are preferentially in the direction of our line of sight. The 90° inclination of Vela X-1 places the obscuring material in the orbital plane.

A reanalysis of the *Einstein* SSS spectra confirms that deviations from the simple neutral absorption model seen in a $\phi \sim 0.19$ spectrum is caused by photoionization, as suggested by Kallman and White (1982). The SSS $\phi \sim 0.75$ spectrum is

similar to the *EXOSAT* basal level absorption spectra taken at this phase. We find that the SSS spectrum is dominated by the scattered component and that this component has Si and S edge structure similar to that observed by Kallman and White (1982). A low-energy excess in the spectra of Vela X-1 has also been reported from *Tenma* observations made in 1983. Nagase *et al.* (1986) modeled the excess with absorption by dense clumps of material with dimensions of a few kilometers partially covering the X-ray source. We find that the X-ray pulsations are greatly reduced in the low-energy excess which is not consistent with the excess coming from partial covering. It is consistent with scattering around a high-density region which would smear out the pulses.

The properties of the base level absorption from Vela X-1 are similar to these found from 4U 1700−37 (HWK). From both sources the spectra at later orbital phases show high absorption and a strong excess below 4 keV. The modeling of the absorption profile over one orbital period of 4U 1700−37 shows that a dense gas stream originating at the surface of the main star and trailing the X-ray source is responsible for the higher absorption after phase 0.6 (HWK). The lack of contiguous phase coverage and the erratic increases in $N_{\rm H}$ prevent a similar modeling for Vela X-1. However the increase in the basal $N_{\rm H}$ at later orbital phase suggests the existence of a similar gas stream. The flux in the scattered component is similar in both cases. The companion of Vela X-1 rotates with a period of 19 days, about twice the orbital period (Sadakane *et al.* 1985; Boynton *et al.* 1984, 1986). Any gas stream from the inner Lagrangian Point will probably trail the neutron star without being accreted (Petterson 1978).

The brightest flare showed an intensity increase by a factor of 4 and was preceded ~35 minutes and ~146 minutes earlier by two large increases in hardness ratio. The flare itself requires an increase in mass accretion rate caused by a density enhancement in the outward flowing wind. This particular observation was made at an orbital phase of 0.86 which would be favorable for viewing the X-ray source through a shell-like enhancement before it reaches the X-ray source. The time delay will depend on the wind velocity and viewing geometry. For a phase of 0.86 the shell crosses first the line of sight at a distance of $1.35R_*$ from the primary star center. With the separation of the neutron star and primary star of $1.71R_*$ the time delays of 146 minutes and 35 minutes give an average wind velocity of ~900 km s^{-1} and ~3800 km s^{-1}, respectively. The former is consistent with a Castor, Abbott, and Klein (1975) velocity law $v_w = v_\infty(1 - 1/r_*)^\beta$ where the wind velocity v_w is at a distance r_* in stellar radii given by the terminal velocity v_∞ (1700 km s^{-1}; Dupree *et al.* 1980) for $\beta \sim 0.39$ (see HWK). The larger value exceeds the terminal velocity. The second increase in hardness ratio may be associated with a small flare in intensity at 22:36, corresponding to a time delay also of 146 minutes (Fig. 1) and indicates a shell whose azimuthal extent only partially reached the neutron star.

The erratic increases in $N_{\rm H}$ up to a factor of 10 from Vela X-1 are not seen from 4U 1700−37. The dip on 1985 May 5 and the entire May 7 (phase 0.5) observation show exceptionally high absorption of 7×10^{23} H cm^{-2}. This is also evident in the 1983 *Tenma* spectra (Sato *et al.* 1986) where variations in column density by up to a factor of 10 are seen at the same orbital phase on different cycles. The detection of a relatively constant scattered component during these intervals suggests the material is confined to the orbital plane. The fact that these high $N_{\rm H}$ intervals are quite long lived suggests that the material orbits the neutron star and may indicate the formation of a tenuous accretion disk. The erratic variations in the pulse period from intervals of rapid spin up to spin down suggest that the wind flow around the neutron star can change direction and require substantial torques on the neutron star that in themselves suggests the occasional presence of a disk (White 1985). Two-dimensional hydrocalculations by Taam and Fryxell (1988) and Fryxell and Taam (1988) show that the wind flow past the neutron star is unstable and can flow in a complex fashion occasionally settling into a disklike pattern, swirling in either direction. The dynamic intervals of high $N_{\rm H}$ may represent times when the flow around the neutron star is disklike. This predicts that the intervals of maximum spinup and spindown occur when the $N_{\rm H}$ is a maximum. Further high-sensitivity studies of the pulse period history should search for such a correlation.

We thank the other members of the *EXOSAT Observatory* team for their support. Tim Kallman is thanked for useful discussions.

REFERENCES

Boynton, P. E., Deeter, J. E., Lamb, F. E., and Zylstra, G. 1986, *Ap. J.*, **307**, 545.
Boynton, P. E., Deeter, J. E., Lamb, F. E., Zylstra, G., Pravdo, S. H., White, N. E., Wood, K. S., and Yentis, D. J. 1984, *Ap. J. (Letters)*, **283**, L53.
Castor, J. I., Abbott, D. C., and Klein, R. I. 1975, *Ap. J.*, **195**, 157.
Conti, P. S. 1978, *Astr. Ap.*, **63**, 225.
Dupree, A. K., *et al.* 1980, *Ap. J.*, **238**, 969.
Forman, W., *et al.* 1973, *Ap. J. (Letters)*, **182**, L103.
Fryxell, B. A., and Taam, R. E. 1988, *Ap. J.*, **335**, 862.
Haberl, F., White, N. E., and Kallman, T. 1989, *Ap. J.*, **343**, 409 (HWK).
Kallman, T. R., and White, N. E. 1982, *Ap. J. (Letters)*, **261**, L35.
Kitamoto, S., Miyamoto, S., Tanaka, Y., Ohashi, T., Tawara, Y., and Nagakawa, M. 1984, *Pub. Astr. Soc. Japan*, **36**, 731.
Krolik, J. H., and Kallman, T. R. 1984, *Ap. J.*, **286**, 366.
McClintock, J. E., *et al.* 1976, *Ap. J. (Letters)*, **206**, L99.
Morrison, R., and McCammon, D. 1983, *Ap. J.*, **270**, 119.
Nagase, F., Hayakawa, S., Sato, N., Masai, K., and Inoue, H. 1986, *Pub. Astr. Soc. Japan*, **38**, 547.
Petterson, J. A. 1978, *Ap. J.*, **224**, 625.
Rappaport, S., Joss, P. C., and McClintock, J. E. 1976, *Ap. J. (Letters)*, **206**, L105.
Sadakane, K., Hirata, R., Jugaku, J., Kondo, Y., Matsuoka, M., Tanaka, Y., and Hammerschlag-Hensberge, G. 1985, *Ap. J.*, **288**, 284.
Sato, N., *et al.* 1986, *Pub. Astr. Soc. Japan*, **38**, 731.
Taam, R. E., and Fryxell, B. A. 1988, *Ap. J. (Letters)*, **327**, L73.
Tarter, C. B., Tucker, W. H., and Salpeter, E. E. 1969, *Ap. J.*, **156**, 943.
Watson, M. G., and Griffiths, R. E. 1977, *M.N.R.A.S.*, **178**, 513.
White, N. E. 1985, in *Interacting Binaries*, ed. M. L. Eggleton and J. E. Pringle (Dordrecht: Reidel), p. 249.
White, N. E., and Peacock, A. 1988, in *Mem. Soc. Astr. Italiana*, **53**, 7.
White, N. E., Swank, J. H., and Holt, S. S. 1983, *Ap. J.*, **270**, 711.

FRANK HABERL and NICK E. WHITE: *EXOSAT Observatory*, Astrophysics Division, Space Science Department, ESTEC, Postbus 299, 2200AG Noordwijk, The Netherlands